タの無数の組み合わせが可能であるが，そのすべてをボランティアで撮像して評価するのは不可能である。最も望ましいコントラストが得られるまでパラメータを変化させて試行錯誤するために多大な労力を必要とし，真に最適化されたかどうかの確認も難しい。本ツールを使えば，実際に撮像することなく，目的とするコントラストとなる撮像パラメータを推定できる。従って，その推定された撮像パラメータの近傍のみの値を用いて実際に撮像し評価をすることにより，効率的に求める撮像条件を得ることができる。実際のMRI装置では，RFパルスの不完全性や撮像スライス内の位置によるフリップ角の変化などにより，信号強度が我々の採用した理論式通りにならないので，推定されたパラメータは，そのまま使うことはできないが，ファントムやボランティアによる撮像で最適化をする際の撮像条件の目安として有用と考える。

一方，独立変数である生体組織の特性が十分には知られておらず，このツールを真に有用なものとするためにも，今後さらに生体組織の特性を明らかにしていく研究が必要である。また，高速スピンエコー法のマルチスライスのイメージングではmagnetization transfer（MT）効果が，画像のコントラストに大きく影響する[23]。この影響は，今回のツールでは，適当に組織の緩和時間を変えることで対応する他はないが，MTの影響で見かけの緩和時間がどの程度変化するかは，測定しないと分からない面がある。この点は今後の改善を要する問題である。

謝　辞

本研究は，厚生労働科学研究費補助金 厚生科学基盤研究分野 医療機器開発推進研究（ナノメディシン研究）の助成を受けたものである。

Appendix

turbo-FLASHシーケンスにおいて，m_0を熱平衡状態の縦磁化，TIを反転時間，T_1を縦緩和時間，TRをイメージング用RFパルスの繰り返し時間，$a \equiv \cos(\mathrm{FA})e^{-\frac{TR}{T_1}}$とすると，$m$回目のRFパルス直前の縦磁化は次の式で与えられる[6]。

$$m_0\left(a^{m-1}\left(1-\left(1+\frac{m_{01}}{m_0}\right)e^{-\frac{TI}{T_1}}\right)+\frac{(1-a^{m-1})\left(1-e^{-\frac{TR}{T_1}}\right)}{1-a}\right)$$

ここで，m_{01}は定常状態となったときの反転パルス直前の縦磁化で，mtxを位相エンコード方向のマトリックス数（これは単位シーケンス当たりのイメージング用のRFパルスの総数に等しい），TDをイメージング用RFパルスによる信号採取が全て終了してから次の反転パルスまでの時間とすると，次の式が成り立つ。

$$m_0\left[1-\left(1-a^{mtx}\left(1-(1+\frac{m_{01}}{m_0})e^{-\frac{TI}{T_1}}\right)-\frac{(1-a^{mtx})\left(1-e^{-\frac{TR}{T_1}}\right)}{1-a}\right)e^{-\frac{TD}{T_1}}\right]=m_{01}$$

これをm_{01}について解くと，次の式が得られる。

$$m_{01}=m_0\frac{\left(e^{\frac{TR}{T_1}}-a\left(e^{\frac{TR}{T_1}}-1\right)-e^{-\frac{TR}{T_1}}\right)-a^{mtx}\left(a\left(1-e^{-\frac{TI}{T_1}}\right)+e^{-\frac{TI}{T_1}}-e^{-\frac{TR}{T_1}}\right)}{(1-a)\left(e^{\frac{TR}{T_1}}+a^{mtx}e^{-\frac{TI}{T_1}}\right)}$$

文　献

1) Haacke, E.M., Brown, R.W., Thompson, M.R., Venkatesan, R.: Magnetic Resonance Imaging: Physical Principles and Sequence Design, 1st ed., Wiley-Liss, New York, 1999
2) Kneeland, J.B., Knowles, R.J., Cahill, P.T.: Multi-section multi-echo pulse magnetic resonance techniques: optimization in a clinical setting, Radiology, **155**, 159-162, 1985
3) McVeigh, E.R., Henkelman, R.M., Bronskill, M.J.: Optimization of survey protocols for MRI, Magn. Reson. Med., **13**, 177-191, 1990
4) Epstein, F.H., Mugler, 3rd, J.P., Brookeman, J.R.: Optimization of parameter values for complex pulse sequences by simulated annealing: application to 3D

MP-RAGE imaging of the brain, Magn. Reson. Med., **31**, 164-177, 1994

5) Mugler, 3rd, J.P., Brookeman, J.R. : Three-dimensional magnetization-prepared rapid gradient-echo imaging (3D MP RAGE), Magn. Reson. Med., **15**, 152-157, 1990

6) Tamura, H., Yanagawa, I., Hikichi, T., Matsumoto, K., Takahashi, S., Sakamoto, K. : T1 measurements with clinical MR units, Tohoku J. Exp. Med., **175**, 249-267, 1995

7) Meara, S.J., Barker, G.J. : Evolution of the longitudinal magnetization for pulse sequences using a fast spin-echo readout : application to fluid-attenuated inversion-recovery and double inversion-recovery sequences, Magn. Reson. Med., **54**, 241-245, 2005

8) Scheffler, K., Lehnhardt, S. : Principles and applications of balanced SSFP techniques, Eur. Radiol., **13**, 2409-2418, 2003

9) Haase, A. : Snapshot FLASH MRI. Applications to T1, T2, and chemical-shift imaging, Magn. Reson. Med., **13**, 77-89, 1990

10) Whittall, K.P., MacKay, A.L., Graeb, D.A., Nugent, R.A., Li, D.K., Paty, D.W. : In vivo measurement of T2 distributions and water contents in normal human brain, Magn. Reson. Med., **37**, 34-43, 1997

11) Wansapura, J.P., Holland, S.K., Dunn, R.S., Ball, W.S. Jr. : NMR relaxation times in the human brain at 3.0 tesla, J. Magn. Reson. Imaging, **9**, 531-538, 1999

12) Gelman, N., Ewing, J.R., Gorell, J.M., Spickler, E.M., Solomon, E.G. : Interregional variation of longitudinal relaxation rates in human brain at 3.0 T : relation to estimated iron and water contents, Magn. Reson. Med., **45**, 71-79, 2001

13) Stanisz, G.J., Odrobina, E.E., Pun, J., Escaravage, M., Graham, S.J., Bronskill, M.J., Henkelman, R.M. : T1, T2 relaxation and magnetization transfer in tissue at 3T, Magn. Reson. Med., **54**, 507-512, 2005

14) Knight, R.A., Dereski, M.O., Helpern, J.A., Ordidge, R.J., Chopp, M. : Magnetic resonance imaging assessment of evolving focal cerebral ischemia. Comparison with histopathology in rats, Stroke, **25**, 1252-1261, 1994

15) Schwarcz, A., Ursprung, Z., Berente, Z., Bogner, P., Kotek, G., Meric, P., Gillet, B., Beloeil, J.C., Dóczi, T. : In vivo brain edema classification : New insight offered by large b-value diffusion-weighted MR imaging, J. Magn. Reson. Imaging, **25**, 26-31, 2007

16) Chabert, S., Scifo, P. : Diffusion signal in magnetic resonance imaging : origin and interpretation in neurosciences, Biol. Res., **40**, 385-400, 2007

17) Tamura, H., Kurihara, N., Machida, Y., Nishino, A., Shimosegawa, E. : How does water diffusion in human white matter change following ischemic stroke ?, Magn. Reson. Med. Sci., **8**, 121-134, 2009

18) Demarco, J.K., Rutt, B.K., Clarke, S.E. : Carotid plaque characterization by magnetic resonance imaging : review of the literature, Top. Magn. Reson. Imaging, **12**, 205-217, 2001

19) Morrisett, J., Vick, W., Sharma, R., Lawrie, G., Reardon, M., Ezell, E., Schwartz, J., Hunter, G., Gorenstein, D. : Discrimination of components in atherosclerotic plaques from human carotid endarterectomy specimens by magnetic resonance imaging ex vivo, Magn. Reson. Imaging, **21**, 465-474, 2003

20) Pessanha, B.S., Potter, K., Kolodgie, F.D., Farb, A., Kutys, R., Mont, E.K., Burke, A.P., O'leary, T.J., Virmani, R. : Characterization of intimal changes in coronary artery specimens with MR microscopy, Radiology, **241**, 107-115, 2006

21) Qiao, Y., Ronen, I., Viereck, J., Ruberg, F.L., Hamilton, J.A. : Identification of atherosclerotic lipid deposits by diffusion-weighted imaging, Arterioscler. Thromb. Vasc. Biol., **27**, 1440-1446, 2007

22) Tamura, H. : http://www.nidi.med.tohoku.ac.jp/web Mathematica/MRI_Notes/, 2010

23) Turner, R., Oros-Peusquens, A.M., Romanzetti, S., Zilles, K., Shah, N.J. : Optimised in vivo visualisation of cortical structures in the human brain at 3 T using IR-TSE, Magn. Reson. Imaging, **26**, 935-942, 2008

J Neurosurg 113:890–896, 2010

Assessment of necrotic core with intraplaque hemorrhage in atherosclerotic carotid artery plaque by MR imaging with 3D gradient-echo sequence in patients with high-grade stenosis

Clinical article

Tomohito Hishikawa, M.D.,[1] Koji Iihara, M.D.,[1] Naoaki Yamada, M.D.,[2] Hatsue Ishibashi-Ueda, M.D.,[3] and Susumu Miyamoto, M.D.[1]

Departments of [1]Neurosurgery, [2]Radiology, and [3]Pathology, National Cardiovascular Center, Osaka, Japan

Object. The aim of this study was to assess the histopathological differences between advanced atherosclerotic carotid artery (CA) plaques with signal hyperintensity on T1-weighted MR images and those without, focusing on necrotic core size and intraplaque hemorrhage (IPH).

Methods. Thirty-five patients scheduled for carotid endarterectomy underwent preoperative CA MR imaging using 3D inversion-recovery-based T1-weighted imaging (magnetization-prepared rapid acquisition gradient-echo [MPRAGE]). The signal intensity of the CA plaque on MPRAGE sequences was classified as "high" when the intensity was more than 200% that of adjacent muscle. A total of 96 axial MR images obtained in 35 patients were compared with corresponding histological sections from 36 excised specimens. The area of the necrotic core in histological sections was compared between specimens with and without high signal intensity on MPRAGE sequences. The IPH was histopathologically graded according to the size of the area positive for glycophorin A as revealed by immunohistochemical staining. The difference between plaques with and without high signal intensity was investigated with respect to the degree of IPH. The relationship of the severity of IPH to size of the necrotic core was also evaluated.

Results. The area of the necrotic core in plaques with high signal intensity on MPRAGE sequences was significantly larger than that in plaques without high signal intensity (median 51.2% [interquartile range 43.3–66.8%] vs 49.0% [33.2–57.6%], $p = 0.029$). Carotid artery plaques with high signal intensity had significantly more severe IPH than plaques with lower signal intensity ($p < 0.0001$). The severity of IPH was significantly associated with the size of the necrotic core ($p < 0.0001$).

Conclusions. Atherosclerotic CA plaques with high signal intensity on MPRAGE sequences had large necrotic cores with IPH in patients with high-grade stenosis; MPRAGE is useful for the evaluation of CA plaque progression.
(DOI: 10.3171/2010.3.JNS091057)

Key Words • **carotid artery stenosis** • **intraplaque hemorrhage** • **MR imaging** • **necrotic core**

The prophylactic effectiveness of CEA in patients with more than a certain degree of arterial stenosis has been proven in several randomized multicenter trials.[7,8,11,21] Although the degree of lumen narrowing is a significant risk factor in stroke, the role of vulnerable CA plaque has recently been emphasized,[20] and some reports have demonstrated that episodes of cerebral ischemia in patients with CA lesions are not restricted to cases with severe stenosis.[3,10,24] The type of vulnerable plaque that is most prone to rupture is characterized by a large necrotic core, a thin fibrous cap (< 65 μm thick), and widespread macrophage infiltration within the fibrous cap.[31] In addition, the role of IPH in the vulnerability of CA plaques has been emphasized by many investigators.[6,17,26,28,29,34]

Magnetic resonance imaging is well suited for CA plaque evaluation in a clinical setting because it is noninvasive and widely available, provides excellent soft tissue contrast, and does not involve ionizing radiation. In response to reports demonstrating the close association of IPH with cerebral ischemic events,[26] many authors have recently emphasized the value of IPH detection by MR imaging and have demonstrated the clinical usefulness of this noninvasive modality.[1,6,13,17,28,29,33]

Our institute has routinely performed CA plaque MR imaging using 3D inversion-recovery-based T1-weighted sequences (MPRAGE) before interventions for CA stenosis. Yamada et al.[33] demonstrated that CA plaque with high signal intensity on MPRAGE sequences was significantly associated with previous ipsilateral ischemic events in patients with moderate and severe stenosis. In that report,

Abbreviations used in this paper: CA = carotid artery; CEA = carotid endarterectomy; ICA = internal carotid artery; IPH = intraplaque hemorrhage; IQR = interquartile range; MPRAGE = magnetization-prepared rapid acquisition gradient echo.

This article contains some figures that are displayed in color online but in black and white in the print edition.

CA plaque signal intensity on greater than 200% that of adjacent muscles was defined as high and the chi values for interobserver and intraobserver agreement were 0.729 and 0.792, respectively (good agreement).[33] Taking the close association of MPRAGE signal intensity (using a threshold of 200% of the intensity of adjacent muscles) with symptomatology into consideration, we sought to determine the histopathological differences between CA plaques with and without high signal intensity as the next stage of investigation. The aim of this study was to retrospectively assess the vulnerability of CA plaques, focusing on differences in necrotic core area and degree of IPH between plaques that are associated with high signal intensity on MPRAGE sequences and those that are associated with lower signal intensity (< 200% of the intensity of adjacent muscle tissue).

Methods

Study Population

Thirty-five patients (32 men, 3 women) with a mean (± SD) age of 69.0 ± 7.8 years who were scheduled for CEA at our institute between May 2006 and March 2007 were included in this study. Patient characteristics were examined retrospectively through a review of the relevant medical records. A total of 36 CEAs for CA stenosis (1 patient had bilateral CA stenosis) were performed, and 36 endarterectomy specimens were analyzed. Twenty patients (57.1%) had a history of ipsilateral ischemic events, including cerebral infarction, transient ischemic attack, and retinal ischemia, within the previous 6 months, and their lesions were defined as symptomatic. The degree of CA stenosis was measured using digital subtraction angiography (17 lesions), 3D CT angiography (17 lesions), or contrast-enhanced MR angiography (2 lesions) according to the method used in the North American Symptomatic Carotid Endarterectomy Trial (NASCET).[9] The criteria for CEA were 70% stenosis or greater for symptomatic cases and 75% stenosis or greater for asymptomatic cases.[12] All 36 endarterectomy specimens were circumferentially removed with the plaque intact.

Magnetic Resonance Imaging Protocol

Imaging was performed using standard neck array and spine array coils in a Magnetom Sonata 1.5-T system (Siemens). Plaque imaging was performed using MPRAGE in the transaxial section with null blood condition (effective inversion time 660 msec; TR 1500 msec) and the water excitation technique to suppress fat signals.[33] Other scanning parameters were as follows: TE 5.0 msec; FOV 180 × 180 mm; matrix 256 × 204; section thickness 1.25 mm; 56 partitions, covering 70 mm around the CA bifurcation; and data acquisition time 5 minutes. The mean interval between MR imaging and CEA was 17.9 ± 20.4 days. In symptomatic patients, the mean duration of time from last symptoms to MR imaging was 16.2 ± 27.0 days.

Image Review and Criteria

The MR images were reviewed by an experienced radiologist (N.Y.) blinded to clinical and pathological data. The signal intensity of plaques on MPRAGE relative to the signal intensity in adjacent muscle (typically the sternocleidomastoid muscle)—referred to in this paper as the relative MPRAGE signal intensity—was calculated in each image at 5-mm intervals extending rostrally along the ICA from the CA bifurcation. Any section of plaque that displayed a signal intensity that was more than 200% that of the adjacent muscle tissue was categorized as having high signal intensity.

Endarterectomy Specimen Processing and Criteria

In symptomatic cases, the mean value of the time from most recent symptoms to CEA was 20.3 ± 28.1 days. The endarterectomy specimens were immediately fixed in Histochoice fixative (Amresco, Inc.) for 48 hours and decalcified with EDTA. Subsequently, they were divided into 5-mm blocks (starting at the CA bifurcation and extending rostrally along the ICA) and embedded in paraffin. From each 5-mm block, a 3-μm section was obtained and stained with H & E and Masson trichrome for histological evaluation. In addition, immunohistochemical testing for glycophorin A was performed to identify IPH (1:200 dilution; Dako). Each section was histopathologically evaluated by an experienced histopathologist (H.I.U.) who was unaware of the MR imaging results. Atheromatous plaques were defined as areas of protrusion into the vascular lumen due to atherosclerosis that were bounded by an internal elastic layer and included fibrous caps. Necrotic core was defined as a core area of atheromatous plaques that consisted of necrotic macrophages, cholesterol crystals, and sometimes hemorrhage. The proportion of the necrotic core area to the total plaque area (NC proportion) was measured using a computer-based morphometric system (WinRoof, Mitani Co.). As an index of the degree of IPH (IPH score), the ratio of the glycophorin A–positive area to the total plaque area was calculated and the sample was graded according to the following scale: a ratio ≥ 0.40 corresponded to a score of 3; a ratio ≥ 0.20 and < 0.40, a score of 2; a ratio < 0.20, a score of 1.

Correlation of MR Imaging and Histological Specimens

The MR images and histological sections were independently reviewed and evaluated. The relative distance from the CA bifurcation was used as a landmark to match the histological data with the MR images in the longitudinal direction of the artery. Morphological features such as lumen size and shape were also used as a reference landmark.

Statistical Analysis

Quantitative variables are presented as the medians and IQRs. The correlation between the relative MPRAGE signal intensity and the NC proportion or IPH score was assessed by nonparametric analysis of the Spearman rank correlation test. The Mann-Whitney U-test was used to compare the NC proportion in samples with high signal intensity on MPRAGE sequences to the proportion in samples with lower signal intensity. Contingency tables displaying IPH scores and MPRAGE signal intensity

(high vs not high) were generated and analyzed by means of the chi-square test to determine a trend. The relationship of IPH score to NC proportion was assessed through nonparametric analysis using the Kruskal-Wallis test. All statistical analyses were performed with StatView (SAS Institute). Differences were considered to be significant when p values were < 0.05.

Results

A total of 96 histological sections corresponding to MR images from 36 endarterectomy specimens were evaluated in this study. Table 1 shows the baseline characteristics of patients, including demographic variables and risk factors.

Correlation Between Size of Necrotic Core and MPRAGE Signal Intensity

Figure 1 shows a scatterplot of the relative MPRAGE signal intensity and the NC proportion. A significant positive correlation was found between the relative MPRAGE signal intensity and the NC proportion ($p = 0.0032$). The NC proportions in plaques with high signal intensity were significantly larger than those in plaques without high signal intensity (median 51.2% [IQR 43.3–66.8%] vs 49.0% [IQR 33.2–57.6%], $p = 0.029$; Fig. 2).

Relationship Between IPH and MPRAGE Signal Intensity

Figure 3 shows a scatterplot of the relative MPRAGE signal intensity and the IPH score. There was a significant positive correlation between the relative MPRAGE signal intensity and the IPH score ($p < 0.0001$). High signal intensity was seen in images corresponding to 14.3, 25.0, and 64.3% of specimens with IPH scores of 1, 2, and 3, respectively. Higher IPH score was significantly associated with high signal intensity on MPRAGE sequences ($p < 0.0001$; Table 2).

Relationship Between IPH and Necrotic Core

The median values (IQRs) for NC proportion were 32.7% (25.3–47.8%), 45.4% (40.5–54.8%), and 53.1% (47.4–65.6%) for samples with IPH scores of 1, 2, and 3, respectively. Higher IPH scores were significantly associated with larger necrotic cores ($p < 0.0001$; Fig. 4).

Representative Examples

Figures 5 and 6 show the representative appearance of MPRAGE images and histological findings from corresponding specimens.

Discussion

Role of IPH in Plaque Progression

Naghavi et al.[19] proposed the concept of vulnerable patients, along with criteria for defining vulnerable plaques, based on autopsy studies of coronary arteries. Among their criteria, IPH has recently been emphasized in pathological studies as an important factor in CA plaque progression.[14,15,32] It has been reported that necrotic core enlargement is crucial for plaque rupture and that increased free cholesterol within the necrotic core is closely associated with lesion instability.[32] Concerning the derivation of free cholesterol, it is generally accepted that apoptotic macrophages are an efficient source of free cholesterol in plaques,[27] although Kolodgie and colleagues[15,32] have demonstrated new lines of evidence suggesting that erythrocyte membranes contribute a significant amount of the free cholesterol in coronary plaques. Nuotio et al.[22] also reported that IPH could play a role in the vulnerability of symptomatic CA plaques by contributing to lipid accumulation and inducing adipophilin (an adipose differentiation-related protein) and further increasing lipid accumulation by preventing lipid efflux. From a symptomatological point of view, Lusby et al.[16] demonstrated that a history of multiple hemorrhage (hemorrhages at various ages) was seen in 81% of patients with symptoms of cerebral ischemia associated with atherosclerotic CA stenosis.

TABLE 1: Summary of demographic and clinical characteristics in 35 patients*

Characteristic	Value
symptomatic lesions	20 (57)
mean degree of stenosis (%)	80 ± 10
mean age in yrs	69 ± 8
female sex	3 (9)
hypertension	24 (69)
diabetes mellitus	15 (43)
hyperlipidemia	19 (54)
cigarette smoking	20 (57)

* Values represent numbers of patients (%) unless otherwise indicated. Means are presented ± SDs.

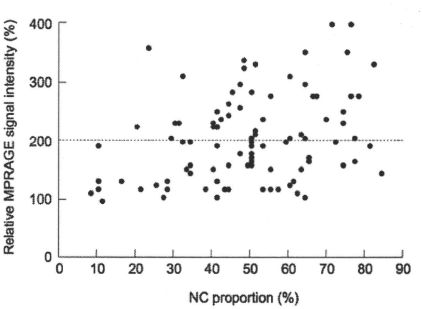

FIG. 1. Scatterplot showing the signal intensity of plaques on MPRAGE sequences relative to the signal intensity in adjacent muscle (relative MPRAGE signal intensity) and the proportion of the necrotic core (NC) area to the total plaque area (NC proportion) as established by pathological examination of specimens. The *broken horizontal line* indicates the level of 200% MPRAGE proportion, the threshold for "high" signal intensity in this study.

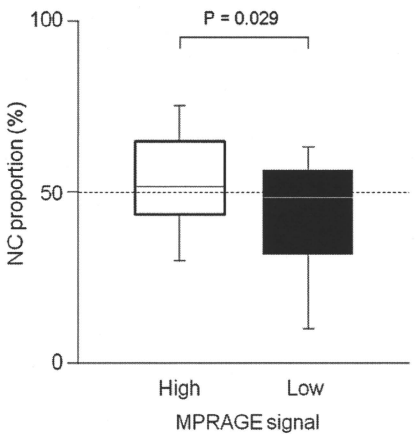

FIG. 2. Box and whisker plot showing the relationship of the NC proportion to MPRAGE signal intensity. The NC proportion in specimens corresponding to imaging studies that showed high signal intensity on MPRAGE sequences was significantly larger than that in specimens that showed lower signal intensity ($p = 0.029$, Mann-Whitney U-test). The *broken horizontal line* is at the level of 50% NC proportion.

The present study demonstrated a significant association of IPH with necrotic core in patients with high-grade CA stenosis. Therefore, the use of a noninvasive and objective modality to detect IPH and to predict subsequent necrotic core expansion in CA plaque could play an important role in assessing plaque vulnerability and in managing patients with CA stenosis in a clinical setting.

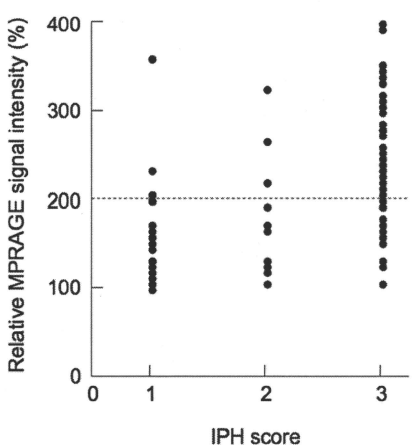

FIG. 3. Scatterplot showing the relative MPRAGE signal intensity and IPH score (1–3). The *broken horizontal line* is at the 200% threshold for high signal intensity.

TABLE 2: Correlation between high signal intensity on MPRAGE sequences in 96 axial MR images and IPH score in corresponding histological sections*

IPH Score	No. of MR Images	Relative Signal Intensity >200%		p Value
		Yes	No	
1	28	4 (14.3)	24 (85.7)	
2	12	3 (25.0)	9 (75.0)	<0.0001
3	56	36 (64.3)	20 (35.7)	

* Signal intensity in CA plaque was assessed relative to that of adjacent muscle tissue, using 200% as the threshold for "high" signal intensity on MPRAGE sequences. Values represent numbers of images, expressed as a percentage of the images in the given score category in parentheses.

Assessment of Carotid Plaque by MPRAGE Sequence

Moody et al.[17] used a T1-weighted magnetization-prepared 3D gradient echo sequence, a technique identical to that used in MPRAGE, to detect complicated plaque by detecting IPH in an in vivo study of CA plaques in symptomatic patients. Bitar et al.[4] recently reported that MR imaging of IPH using a 3D spoiled gradient-echo sequence resulted in strong agreement between imaging and histologic findings. Yamada et al.[33] disclosed significant associations between cerebral ischemic events and MPRAGE hyperintensity according to stenosis severity using 200% of the signal intensity of adjacent muscle as the threshold for high signal intensity and reported the percentages of patients with high signal intensity were 21, 54, and 65% for mild (0–29%), moderate (30–69%), and severe (70–99%) stenosis, respectively. The present study demonstrated that the NC proportion in plaques with high signal intensity on MPRAGE sequences was significantly larger than that in plaques with lower signal intensity, and the severity of IPH was significantly correlated with signal intensity. The hemorrhage-rich larger necrotic core is a pathological basis for the high signal intensity on MPRAGE in these plaques, which has previously been shown to be significantly associated with symptomatology.[33] Also, in the present study, 58% of CAs examined (21 of 36) had high signal intensity on MPRAGE sequences and 58% of the endarterectomy sections (56 of 96) exhibited the highest degree of IPH (score of 3 in our pathological examination). Together with the data from Yamada et al.,[33] the data from this study shows, through the association between MPRAGE signal hyperintensity and high-grade CA stenosis, that IPH has a high prevalence in advanced CA atherosclerotic plaques; our data also raise the possibility that IPH is a major mechanism underlying the progression of stenosis through its stages of severity as well as the expansion of the necrotic core.

The majority of previous reports have used multiple contrast techniques (T1-weighted, T2-weighted, proton-density–weighted, and 3D time-of-flight MR imaging)

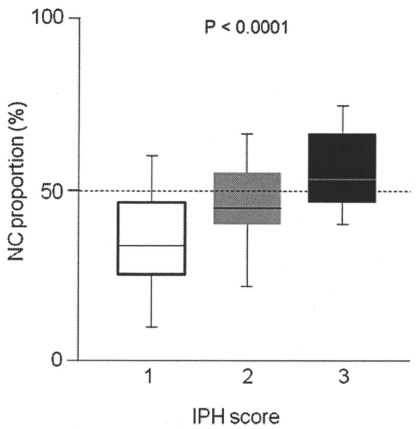

FIG. 4. Box and whisker plot showing the relation of IPH score to NC proportion. Higher IPH scores were significantly associated with higher NC proportion, according to the Kruskal-Wallis test ($p < 0.0001$). The *broken horizontal line* is at the level of 50% NC proportion.

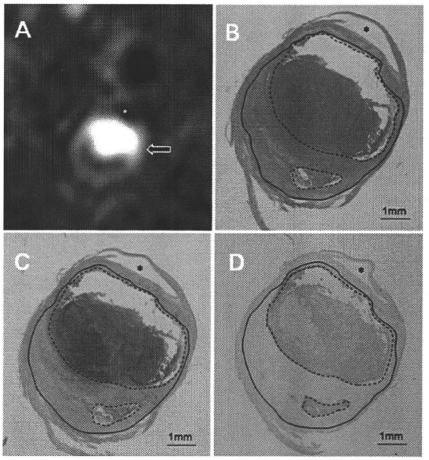

FIG. 5. An example of plaque with high signal intensity. **A:** An MPRAGE image showing the plaque *(arrow)*. **B and C:** Photomicrographs of histological sections showing a large amount of necrotic core with IPH. H & E **(B)** and Masson trichrome **(C)**. **D:** Photomicrograph showing that the necrotic core is strongly positive for glycophorin A. *Asterisks* indicate the ICA lumen. The total plaque area is delineated by a *solid line* and the necrotic core area by a *dotted line*. Bar = 1 mm.

to identify necrotic cores and IPH.[6,13,28,29,34] Saam et al.[25] demonstrated the accuracy and reproducibility of using multicontrast imaging to quantify CA plaque components. On the other hand, the usefulness of single-contrast imaging using a 3D gradient-echo sequence has also been demonstrated.[1,4,17,18,33] This sequence is often employed to identify IPH using a T1-weighted signal alone. In a study comparing the performance of a gradient-echo sequence with that of a spin-echo sequence, the gradient-echo sequence had a higher detection rate for IPH as well as much better interobserver agreement and better image quality.[5] Likewise, Ota et al.[23] reported that the MPRAGE sequence at 3 T had the highest diagnostic capability for the detection and quantification of IPH, in a study comparing it with the fast spin echo and spoiled gradient echo sequences. In the present study, the area over which MPRAGE signal hyperintensity was present in CA plaque was not directly compared with the area of the necrotic core as measured through histopathological analysis. Nevertheless, our data reveal that the areas of high signal intensity on MPRAGE sequences coincide with the hemorrhage-rich large necrotic core. As the interpretation of MPRAGE signal intensity is simple and objective, requiring only a short image acquisition time (5 minutes), this 3D gradient-echo sequence technique is useful in a clinical setting.

As the practice of CA stent placement has rapidly become more prevalent, distal embolic complications during the procedure have become an important clinical issue. A report on the use of a filter protection device during CA stent placement in Japan revealed that disturbed blood flow presumably due to the blockage of the filter pores by plaque was observed in 40.0% of cases (slow flow in 26.7%, no flow in 13.3%).[30] Angeneli et al.[2] collected the embolized debris caught in such a filter and performed histopathological analysis on it; they reported that the collected debris consisted predominantly of thrombotic material, foam cells, and cholesterol clefts. The use of MPRAGE for CA plaque analysis before CA stent placement could be useful in predicting the risk of embolic complication and blood flow disturbances and could aid in selecting suitable distal protection devices.

Study Limitations

First, we used immunohistochemical staining for glycophorin A as a marker of IPH. Glycophorin A is a protein specific to erythrocytes that facilitates anion exchange; it is also an indicator of previous hemorrhage.[15] Although high signal intensity on MPRAGE sequences was associated with the detection of previous hemorrhages by glycophorin A, the signal hyperintensity may not be related to fresh thrombi or hemorrhages. In fact, in this study, a few endarterectomy sections with fresh thrombi revealed only lower-intensity signals. Because fresh thrombi play a crucial role in the pathogenesis of stroke,[26] it is important to detect them and to accurately classify IPH; thus, if MPRAGE is to become a useful technique, we must develop sequences that can detect fresh thrombi and also measure the age of IPH lesions. Second, because the patients included in this study had been selected as candidates for CEA based on the criteria of our institute,[12]

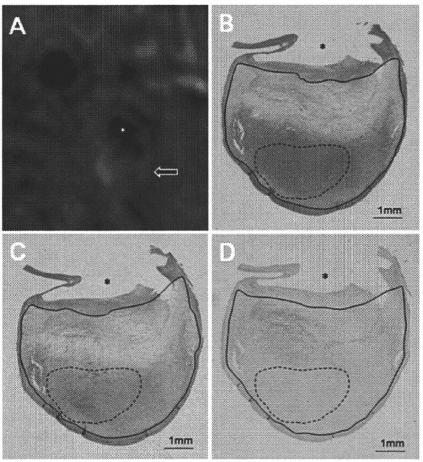

FIG. 6. An example of plaque with lower signal intensity. **A:** An MPRAGE image showing the plaque *(arrow)*. **B and C:** Photomicrographs of ICA sections show the plaque is mainly consisted of fibrous tissue and focal calcification. H & E **(B)** and Masson trichrome **(C)**. **D:** Photomicrograph showing that the plaque is only lightly stained for glycophorin A. *Asterisks* indicate the ICA lumen. The total plaque area is delineated by a *solid line* and the necrotic area by a *dotted line*. Bar = 1 mm.

pathological examination and MR imaging analysis in this study were restricted to patients with high-grade stenosis. Yet the relative risk of ipsilateral ischemia according to MPRAGE signal intensity was reported to be the highest in the moderate-stenosis group.[33] In future studies of MPRAGE, it would be better to investigate the pathological differences between patients with moderate stenosis and high signal intensity and those with moderate stenosis and lower signal intensity.

Conclusions

We demonstrated that in CA plaque with high-grade stenosis, high signal intensity on MPRAGE sequences (> 200% increase relative to signal intensity in adjacent muscle tissue) indicates larger necrotic cores and more severe degrees of IPH than lower signal intensity. We also found that IPH is closely associated with necrotic core expansion in advanced CA plaque. These results indicate that MPRAGE, a T1-weighted imaging technique, can accurately reveal plaque progression in conjunction with IPH in patients with high-grade stenosis.

Disclosure

The authors report no conflict of interest concerning the materials or methods used in this study or the findings specified in this paper.

Author contributions to the study and manuscript preparation include the following. Conception and design: T Hishikawa, K Iihara. Acquisition of data: N Yamada, H Ishibashi-Ueda. Reviewed final version of the manuscript and approved it for submission: T Hishikawa, K Iihara, N Yamada, H Ishibashi-Ueda, S Miyamoto. Study supervision: S Miyamoto.

References

1. Altaf N, MacSweeney ST, Gladman J, Auer DP: Carotid intraplaque hemorrhage predicts recurrent symptoms in patients with high-grade carotid stenosis. **Stroke 38:**1633–1635, 2007
2. Angelini A, Reimers B, Della Barbera M, Saccà S, Pasquetto G, Cernetti C, et al: Cerebral protection during carotid artery stenting: collection and histopathologic analysis of embolized debris. **Stroke 33:**456–461, 2002
3. Barnett HJ, Taylor DW, Eliasziw M, Fox AJ, Ferguson GG, Haynes RB, et al: Benefit of carotid endarterectomy in patients with symptomatic moderate or severe stenosis. The North American Symptomatic Carotid Endarterectomy Trial Collaborators. **N Engl J Med 339:**1415–1425, 1998
4. Bitar R, Moody AR, Leung G, Symons S, Crisp S, Butany J, et al: In vivo 3D high-spatial-resolution MR imaging of intraplaque hemorrhage. **Radiology 249:**259–267, 2008
5. Cappendijk VC, Cleutjens KBJM, Heeneman S, Schurink GWH, Welten RJTJ, Kessels AGH, et al: In vivo detection of hemorrhage in human atherosclerotic plaques with magnetic resonance imaging. **J Magn Reson Imaging 20:**105–110, 2004
6. Chu B, Kampschulte A, Ferguson MS, Kerwin WS, Yarnykh VL, O'Brien KD, et al: Hemorrhage in the atherosclerotic carotid plaque: a high-resolution MRI study. **Stroke 35:**1079–1084, 2004
7. European Carotid Surgery Trialists' Collaborative Group: MRC European Carotid Surgery Trial: interim results for symptomatic patients with severe (70-99%) or with mild (0-29%) carotid stenosis. European Carotid Surgery Trialists' Collaborative Group. **Lancet 337:**1235–1243, 1991
8. Executive Committee for the Asymptomatic Carotid Atherosclerosis Study: Endarterectomy for asymptomatic carotid artery stenosis. **JAMA 273:**1421–1428, 1995
9. Fox AJ: How to measure carotid stenosis. **Radiology 186:**316–318, 1993
10. Golledge J, Greenhalgh RM, Davies AH: The symptomatic carotid plaque. **Stroke 31:**774–781, 2000
11. Halliday A, Mansfield A, Marro J, Peto C, Peto R, Potter J, et al: Prevention of disabling and fatal strokes by successful carotid endarterectomy in patients without recent neurological symptoms: randomised controlled trial. **Lancet 363:**1491–1502, 2004
12. Iihara K, Murao K, Sakai N, Yamada N, Nagata I, Miyamoto S: Outcome of carotid endarterectomy and stent insertion based on grading of carotid endarterectomy risk: a 7-year prospective study. **J Neurosurg 105:**546–554, 2006
13. Kampschulte A, Ferguson MS, Kerwin WS, Polissar NL, Chu B, Saam T, et al: Differentiation of intraplaque versus juxtaluminal hemorrhage/thrombus in advanced human carotid atherosclerotic lesions by in vivo magnetic resonance imaging. **Circulation 110:**3239–3244, 2004
14. Kolodgie FD, Burke AP, Nakazawa G, Cheng Q, Xu X, Virmani R: Free cholesterol in atherosclerotic plaques: where does it come from? **Curr Opin Lipidol 18:**500–507, 2007
15. Kolodgie FD, Gold HK, Burke AP, Fowler DR, Kruth HS, Weber DK, et al: Intraplaque hemorrhage and progression of coronary atheroma. **N Engl J Med 349:**2316–2325, 2003
16. Lusby RJ, Ferrell LD, Ehrenfeld WK, Stoney RJ, Wylie EJ: Carotid plaque hemorrhage. Its role in production of cerebral ischemia. **Arch Surg 117:**1479–1488, 1982

17. Moody AR, Murphy RE, Morgan PS, Martel AL, Delay GS, Allder S, et al: Characterization of complicated carotid plaque with magnetic resonance direct thrombus imaging in patients with cerebral ischemia. **Circulation 107:**3047–3052, 2003
18. Murphy RE, Moody AR, Morgan PS, Martel AL, Delay GS, Allder S, et al: Prevalence of complicated carotid atheroma as detected by magnetic resonance direct thrombus imaging in patients with suspected carotid artery stenosis and previous acute cerebral ischemia. **Circulation 107:**3053–3058, 2003
19. Naghavi M, Libby P, Falk E, Casscells SW, Litovsky S, Rumberger J, et al: From vulnerable plaque to vulnerable patient: a call for new definitions and risk assessment strategies: Part I. **Circulation 108:**1664–1672, 2003
20. Nighoghossian N, Derex L, Douek P: The vulnerable carotid artery plaque: current imaging methods and new perspectives. **Stroke 36:**2764–2772, 2005
21. North American Symptomatic Carotid Endarterectomy Trial Collaborators: Beneficial effect of carotid endarterectomy in symptomatic patients with high-grade carotid stenosis. **N Engl J Med 325:**445–453, 1991
22. Nuotio K, Isoviita PM, Saksi J, Ijäs P, Pitkäniemi J, Sonninen R, et al: Adipophilin expression is increased in symptomatic carotid atherosclerosis: correlation with red blood cells and cholesterol crystals. **Stroke 38:**1791–1798, 2007
23. Ota H, Yarnykh VL, Ferguson MS, Underhill HR, DeMarco JK, Oikawa M, et al: Comparison between three T1-weighted sequences for detection and area measurement of intraplaque hemorrhage in carotid atherosclerotic plaque imaging at 3 tesla. **Proc Intl Soc Mag Reson Med 17:**605, 2009 (Abstract)
24. Rothwell PM, Gutnikov SA, Warlow CP: Reanalysis of the final results of the European Carotid Surgery Trial. **Stroke 34:**514–523, 2003
25. Saam T, Ferguson MS, Yarnykh VL, Takaya N, Xu D, Polissar NL, et al: Quantitative evaluation of carotid plaque composition by in vivo MRI. **Arterioscler Thromb Vasc Biol 25:**234–239, 2005
26. Spagnoli LG, Mauriello A, Sangiorgi G, Fratoni S, Bonanno E, Schwartz RS, et al: Extracranial thrombotically active carotid plaque as a risk factor for ischemic stroke. **JAMA 292:**1845–1852, 2004
27. Tabas I: Consequences of cellular cholesterol accumulation: basic concepts and physiological implications. **J Clin Invest 110:**905–911, 2002
28. Takaya N, Yuan C, Chu B, Saam T, Polissar NL, Jarvik GP, et al: Presence of intraplaque hemorrhage stimulates progression of carotid atherosclerotic plaques: a high-resolution magnetic resonance imaging study. **Circulation 111:**2768–2775, 2005
29. Takaya N, Yuan C, Chu B, Saam T, Underhill H, Cai J, et al: Association between carotid plaque characteristics and subsequent ischemic cerebrovascular events: a prospective assessment with MRI—initial results. **Stroke 37:**818–823, 2006
30. Takayama K, Nakagawa H, Iwasaki S, Taoka T, Miyasaka T, Myouchin K, et al: Initial experience of using the filter protection device during carotid artery stenting in Japan. **Radiat Med 26:**348–354, 2008
31. Virmani R, Burke AP, Kolodgie FD, Farb A: Pathology of the thin-cap fibroatheroma: a type of vulnerable plaque. **J Interv Cardiol 16:**267–272, 2003
32. Virmani R, Kolodgie FD, Burke AP, Finn AV, Gold HK, Tulenko TN, et al: Atherosclerotic plaque progression and vulnerability to rupture: angiogenesis as a source of intraplaque hemorrhage. **Arterioscler Thromb Vasc Biol 25:**2054–2061, 2005
33. Yamada N, Higashi M, Otsubo R, Sakuma T, Oyama N, Tanaka R, et al: Association between signal hyperintensity on T1-weighted MR imaging of carotid plaques and ipsilateral ischemic events. **AJNR Am J Neuroradiol 28:**287–292, 2007
34. Yuan C, Mitsumori LM, Ferguson MS, Polissar NL, Echelard D, Ortiz G, et al: In vivo accuracy of multispectral magnetic resonance imaging for identifying lipid-rich necrotic cores and intraplaque hemorrhage in advanced human carotid plaques. **Circulation 104:**2051–2056, 2001

Manuscript submitted July 13 2009.
Accepted March 1, 2010.
Please include this information when citing this paper: published online April 9, 2010; DOI: 10.3171/2010.3.JNS091057.

Address correspondence to: Tomohito Hishikawa, M.D., Department of Neurological Surgery, Okayama University Graduate School of Medicine and Dentistry, 2-5-1 Shikata-cho, Okayama City, Okayama, 700-8558 Japan. email: t-hishi@md.okayama-u.ac.jp.

Ann Vasc Dis Vol.3, No.1; 2010; pp52–59
© Annals of Vascular Diseases 2010

Online July 21, 2010
doi:10.3400/avd.AVDoa09009

Original Article

Plaque Tissue Components Obtained from De Novo Lesions may Predict Restenosis after Directional Coronary Atherectomy

Kentaro Arakawa,[1]* Hatsue Ishibashi-Ueda,[2] Hiroyuki Hao,[3] Yoshihiko Ikeda,[2] and Atsushi Kawamura[1]

Background: **A part of coronary stenotic lesions treated with directional coronary atherectomy (DCA) occur restenosis several months later. Specimens obtained by first DCA, present the histology of culplit lesions and may predict restenosis after PCI.**

Methods: **The study group comprised 76 patients (male/female 65/11, age 61 ± 11 years). Restenosis, defined as > 50% stenosis diameter by quantitative cineangiography, was present in 26 patients. The other 50 patients (< 50% stenosis) constitute the" no restenosis" group. Inflammatory cells and other atheroma components were planimetrically quantified as a percentage of total tissue area.**

Results: **As regards lymphocytes, neutrophils and smooth muscle cells, the grade of amount of cells did not differ between restenosis group and no restenosis group. The amount of obtained arterial media was similar, too. However, the area occupied by macrophages or calcified fragments was significantly larger in restenosis group than no restenosis group. And there was a tendency toward larger area occupied by cholesterol gruel, thrombus and myxomatous extracellular matrix (ECM) in restenosis group.**

Conclusion: **Rich macrophages infiltration, calcified fragments, cholesterol rich gruel and myxomatous ECM from primary lesions can be predictors of restenosis after DCA, suggesting a possible role in restenotic process after PCI.**

Key words: directional coronary athelectomy, restenosis, percutaneous coronary intervention, atherosclerosis, inflammation

Introduction

The mechanisms involved in the process of restenosis after percutaneous coronary intervention are postulated to include elastic recoil, smooth muscle cells (SMCs) proliferation with extracellular matrix (ECM) production, and remodeling.[1–5]

Directional coronary atherectomy (DCA) is one method of percutaneous coronary intervention (PCI) to remove atherosclerotic lesions from the coronary artery wall. Although the specimens obtained by DCA may not reflect the whole situation of coronary arteries, we can observe the histology of culplit lesions, which consist of multiple thin fragments. Atherectomy specimens in de novo lesions reflect the heterogeneity of features that are found in plaques.

Recently, a lot of reports related to DCA specimens have thrown lights on pathophysiology of coronary arteries. As regards to restenosis in de novo lesions, increased macrophages and lymphocytes, higher BTEB-2 expression to stellate SMCs and elevated immunoreactivity to C-reactive protein (CRP) etc. are reported to be indepen-

[1] *Division of Cardiology, Department of Internal Medicine, National Cardiovascular Center, Suita, Osaka, Japan*
[2] *Division of Pathology, National Cardiovascular Center, Suita, Osaka, Japan*
[3] *Division of Surgical Pathology, Hyogo College of Medicine, Nishinomiya, Hyogo, Japan*

Received:May 3, 2009 Accepted: May 11, 2010
Address for reprint requests to Kentaro Arakawa, MD: Division of Cardiology, Fujisawa Municipal Hospital, 2–5–1, Fujisawa, Fujisawa, Kanagawa 251–8550, Japan
Tel: +81–466–25–3111, Fax: +81–466–25–3545
Email: hiroking@gamma.ocn.ne.jp

dent predictors of restenosis after DCA.[6-10]

To test the hypothesis that the specimens obtained from coronary arteries can predict restenosis after PCI, we quantified plaque tissue components and correlated with angiographic restenosis after DCA in patients with stable angina and acute coronary syndrome.

Methods

Study patients

From January 1993 to March 2006, 172 consecutive DCA procedures were performed at the cardiac catheterization laboratories in National Cardiovascular Center, Osaka, Japan. Patients were required to meet the following criteria, (1) successful DCA of the culprit lesion (> 20% reduction in diameter stenosis and residual diameter stenosis < 50%), (2) without stenting, (3) no previous coronary intervention at the site of the culprit lesion, (4) enough large specimens to evaluate (> 1.5 mm^2) (5) follow-up angiography 1 to 6 months after DCA. 76 patients met the inclusion criteria and constitute the study population. There were 65 men and 11 women, with a mean age of 61 ± 11 years. Restenosis, defined as > 50% stenosis diameter by quantitative cineangiography, was present in 26 patients. The remainder of the 50 patients constitute the "no restenosis" group.

Histological analysis of atherectomy specimen

DCA specimens retrieved from culplit lesions were immediately fixed in 10% buffered formalin solution for 6 hours at 4°C and embedded in paraffin. Sections (4 μm thick) were stained with hematoxylin-eosin, masson's trichrome and elastica van Gieson. Moreover, sub-serial sections were examined immunohistochemistry if necessary. The primary monoclonal antibodies used were anti-CD68 (DAKO, Japan) for macrophages, anti-alpha-smooth musle actin (α-SMA; DAKO, Japan) for SMCs and UCHL-1 (DAKO, Japan) for T-lymphocytes, respectively. Briefly we performed, after deparaffinization, pretreatment of tissues with heat-induced epitope retrieval and blocked endogenous peroxidase activity in 3% hydrogen peroxidase in methanol for 10 minutes. Then the sections were incubated with antibodies. Intervending washes with phosphate-buffered saline were followed by incubation with Envision + (DAKO Japan) for 30 minutes. After further washes, the sections were incubated with 0.05% 3,3' diaminobenzidine containing hydrogen peroxide and counterstained with Meyer's hematoxylin. As the negative control for immunostaining, normal mouse immunoglobulin G was used instead of the primary antibody. Human liver obtained at autopsy was used as positive control.

In the quantitative analysis, immunopositive areas of each cell, such as macrophages, T-lymphocytes, neutrophils or SMCs, and calcified fragments were measured as a percentage of the total tissue area. Areas were counted by a planimetry software (Win roof, Mitani, Japan). Fibrin thrombus and cholesterol gruel were also evaluated as the same method (**Fig. 1**). The occupied area percentage of each inflammatory cell (lymphocytes, neutrophils and macrophages), cholesterol gruel and SMCs (α-SMA positive) to total area were calculated. We compared cases as 4 grades; (0), (1+), (2+) and (3+), indicating no cell, < 10%, from 10% to 50% and > 50%, respectively. The presence of deep arterial wall components (media, adventitia) was analyzed, too. Extracellular matrix (ECM) was classified into two patterns, namely, hyalinized tissue dominant and myxomatous tissue dominant. The former is sclerotic tissue, composed of dense collagen tissue with low cellularity, while the latter is hypercellular tissue, composed of loose connective tissue matrix containing numerous stellate cells, which were positive to α-SMA (**Fig. 2**).

Macrophages and T-lymphocytes in the fibrous cap were evaluated in the same planimetrically quantative analysis manner.

Quantitative measurement of coronary stenosis

The coronary angiograms were recorded, and quantitative coronary analysis was performed by QCA-CMS Ver.5 (Goodman, Nagoya, Japan). Measurements included the minimal lumen diameter (MLD) of the treated coronary segment, the reference diameter, lesion length and percent diameter stenosis. Acute gain was calculated; MLD immediately after DCA minus MLD immediately before DCA.

Statistical analysis

Data are expressed as mean ± standard deviation. Continuous valiables were compared using the unpaired *t* test. Categorical variables were compared using Fisher's exact test. With respect to histological evaluation except deep wall components and ECM, Scheffe's method was used to perform multiple comparisons between 2 groups. Values of $p < 0.05$ were considered significant.

Results

Patients and angiography

The clinical baseline characteristics of 76 patients included in this study are shown in **Table 1**. And angio-

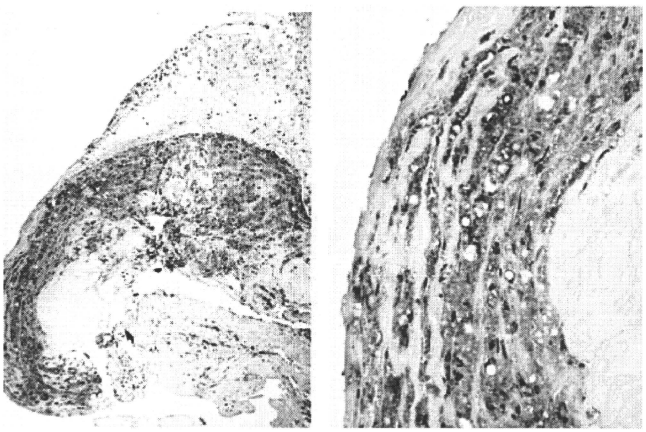

Fig. 1 A representative immunohistochemical staining for CD68 in DCA specimen obtained from a coronary artery, which presented restenosis after 6 months. The area occupied by macrophages is more than 50% (left; × 40, right; × 400 original magnification).

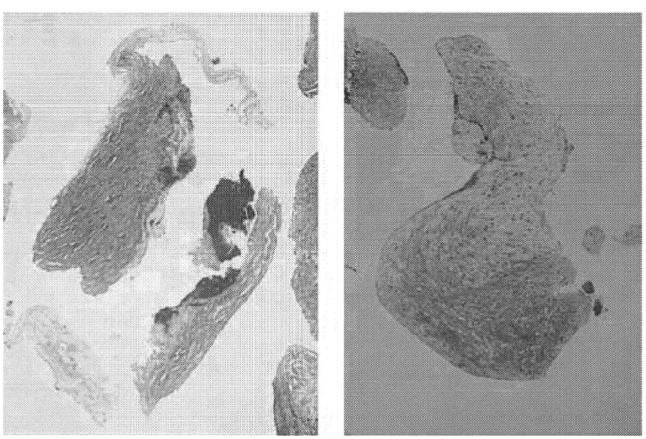

Fig. 2 Left; hyalinized ECM composed of dense collagen tissue (blue part) with low cellularity and organized thrombus (red part). Right; myxomatous ECM composed of a loose connective tissue matrix containing numerous stellate cells (Masson's trichrome staining, × 40, original magnification respectively).

Table 1 Baseline clinical characteristics and coronary angiographic findings

	Restenosis (n = 26)	No-Restenosis (n = 50)	p value
age (yr)	61.7 ± 2.1	60.7 ± 1.5	0.7055
Gender (male n (%))	23 (88%)	42 (84%)	0.5942
Stable AP/ACS n (%)	17/9 (65/35%)	26/24 (52/58%)	0.261
Coronary Risk Factors n (%)			
Hypertension	16 (62%)	31 (62%)	0.9687
Diabetes Mellitus	17 (65%)	29 (98%)	0.5304
Hyperlipidemia	17 (65%)	31 (62%)	0.7712
Smoking	19 (73%)	34 (68%)	0.6458
Family History of CAD	6 (23%)	15 (30%)	0.5180
Drugs n (%)			
Anticoagulant	25 (96%)	46 (92%)	0.4698
Statins	16 (32%)	11 (21%)	0.7712
RCA/LAD/LCX n (%)	3/21/2 (12/81/7%)	1/48/1 (2/96/2%)	0.1039
Reference diameter (mm)	3.30 ± 0.12	3.48 ± 0.09	0.1180
Pre-minimum lesion diameter (mm)	0.62 ± 0.16	0.90 ± 0.11	0.1617
Post-minimum lesion diameter (mm)	2.78 ± 0.89	3.81 ± 0.62	0.0846
Pre persent stenosis (%)	80.3 ± 2.0	80.3 ± 1.4	0.9973
Post persent stenosis (%)	12.6 ± 1.5	13.3 ± 2.1	0.7670
Acute gain (mm)	2.17 ± 0.13	2.36 ± 0.17	0.2193
Lesion length (mm)	8.80 ± 1.89	6.45 ± 0.74	0.0782

Values are mean ± SD or median value (25th to 75th percentile range) or n (%).
AP, angina pectoris; ACS, acute coronary syndrome; CAD, coronary artery disease; yr, years; RCA, right coronary artery; LAD, left coronary artery; LCX left circumflex

graphic characteristics are shown, too. All lesions were located in relatively large proximal coronary segments. There was a trend toward longer lesion and smaller post-MLD in restenosis group, but these did not reach statistical significance. The other baseline clinical and angiographic characteristics were similar between the 2 groups, including acute gain after DCA.

Histologic findings and immunohistochemical findings

The percentage of total area occupied by each inflammatory cell (lymphocytes, neutrophils and macrophages), cholesterol gruel and SMCs (α-SMA positive) were divided into 4 grades; (0), (1+), (2+) and (3+), indicating no cell, < 10%, from 10% to 50% and > 50%, respectively. As regards lymphocytes, neutrophils and SMCs, the grades of occupied area did not differ between restenosis group and no restenosis group. However, the area infiltrated by macrophages was significantly larger in restenosis group than those of no restenosis group ($p = 0.028$). And there was a tendency toward larger area occupied by cholesterol gruel in restenosis group (**Table 2**).

Then, the presence of fibrin thrombus and calcified fragments was also quantified according to the percentage of total tissue area occupied by them; (0), (1+), (2+) and (3+), indicating no fragment, < 10%, from 10% to 20%, and > 20%, respectively. No significant difference in the incidence of fibrin thrombus formation was found between the 2 groups. Calcified fragments were detected in 12 patients of restenosis group, (2+) in 6 patients and (1+) in 6 patients, meanwhile seventy percent of no restenosis group showed no calcified fragments ($p = 0.012$, **Table 2**).

All samples included materials from the intima, some included the media but none showed the presence of the adventitia. The presence of media did not differ between no restenosis group and restenosis group.

As regards ECM, there was a tendency of increased myxomatous tissue in restenosis group. Hyalinized ECM was prominent in no restenosis group, but with no statistical significance (**Table 2**).

The presence of lymphocytes and macrophages in the fibrous cap was also analyzed. Although no significant difference in the presence of lymphocytes was found between the 2 groups, foamy macrophages were detected in

Table 2 Histological analysis of atherectomy specimen

	Restenosis (n = 26)	No-Restenosis (n = 50)	p value
The occupied area grade of total area Grade 0/1/2/3 n (%)			
Inflammatory cells PMNs	10/12/3/1 (38/46/12/4%)	29/17/3/1 (58/34/6/2%)	0.420
Lymphocytes	3/19/3/1 (12/73/12/4 %)	18/24/6/2 (36/48/12/4%)	0.106
Mϕs	2/13/10/1 (8/50/38/4%)	12/28/8/1 (24/56/18/2%)	0.028
Cholesterol gruel	1/16/8/1 (4/61/31/4%)	12/26/9/3(24/52/18/6%)	0.063
α-SMA positive cells	1/12/9/4 (4/46/35/15%)	3/21/19/7 (6/42/38/14%)	0.959
Fibrin thrombus	6/12/6/2 (23/46/23/8 %)	10/23/14/3(20/46/28/6%)	0.958
Calcification	14/6/6/0 (54/23/23/0 %)	35/14/1/0(70/28/2/0%)	0.012
The presence of media n (%)	12 (46%)	26 (52%)	0.629
ECM myxomatous/hyalinized n (%)	14/12 (54/46%)	16/34 (32/68%)	0.065
The presence of inflammatory cells in the fibrous cap n (%)			
Lymphocytes	15 (57%)	25 (50%)	0.523
Mϕs	18 (69%)	23 (46%)	0.051

ECM, extracellular matrix; α-SMA positive cells, alpha smooth muscle actin positive cells; PMNs , polymorphonucler cells; Mϕs, macrophages

18 patients (69%) of restenosis group, with increased tendency than in patients of no restenosis group (**Table 2**).

Discussion

This study shows that the extent of macrophages infiltration in the initial culprit lesion, as documented by immunohistochemistry, and calcified fragments of the atherectomy specimens, are positively associated with coronary restenosis during long-term follow-up after DCA. Additionally, myxomatous ECM and cholesterol gruel may lead to restenosis after DCA.

Inflammatory cells

Experimental and human studies have suggested that inflammatory responses to PCI play an important role in neointimal growth.[8-10] In this study, three inflammatory variables were quantified in the patients' atherectomy tissue: the extent of infiltration of T lymphocytes, which have important immune-regulatory functions in the inflammatory response,[11, 12] macrophages with secretory effector functions and phagocytic reaction to lipid as a foam cell in plaque inflammation, and neutrophils which infiltrate early after endothelial denudation and releases oxygen radicals and proteases.[13, 14]

Our findings indicate that initial plaque inflammation detected by macrophages infiltration contributes to the severity of restenosis despite proliferation of SMCs. And this is consistent with the previous report.[9] This phenomenon may be explained by the fact that after DCA, a substantial amount of the initial atherosclerotic plaque may still persist; hence the persistence of smoldering inflammatory process at the site of intervention cannot be dismissed. Otherwise, Libby et al postulated that angioplasty may induce a change in macrophage phenotype from a resting to an activated state that could be involved in the restenosis process.[13] Macrophage exhibits an early and sustained DNA synthesis in both the intima and the media layers over the first 2 weeks.[17] Macrophage-derived metalloproteinases correlated with SMCs migration from the media into the intima after angioplasty in the rat.[18, 19] Moreover they induce structural disruption of the arterial wall, which triggers thrombosis, the cause of occlusion and the majority of acute vascular events.[20] So, the regulation of inflammatory cells, especially macrophages, is important to prevent coronary restenosis and acute coronary syndrome.

Calcification

The directional atherectomy device is not capable resecting heavily calcified plaque so that only small calcified plaque fragments were typically seen. However, our

results demonstrated that the presence of calcification in obtained sample predicted coronary restenosis after DCA. When PCI was performed to the culplit lesion with calcification, the injury of arterial wall often extend to the medium, followed by thrombus formation, macrophage accumulation and neointimal hyperplasia. In case of DCA, acute gain of calcified lesion after DCA would be limited.

Media

Deep arterial wall excision among DCA was not uncommon; arterial media were present in generally 50% of athrectomy specimens. Deep arterial wall excision is not generally associated with an increased incidence of restenosis.[21, 22] However, this was not supported by the results of another study in which the presence of internal elastic lamina and media in higher percentage of patients of restenosis.[23] It was compatible with the fact that medial SMCs stimulated phenotypic modulation strictly from contractile state to stellate cells. But, it could be postulated that deeper dissection ensuring more complete removal of the atheroma and less residual stenosis after DCA, contribute the larger acute luminal gain in patients without restenosis. This beneficial effect in the form of a larger and smoother lumen after atherectomy appeared to overshadow any adverse event that could occur due to exposure of the media proving a stimulus for greater platelet aggregation and subsequent smooth muscle proliferation.

ECM

The ECM of the vessel wall is a system of acellular substances, providing the connective tissue scaffolding for cellular elements.[24] The ECM consists of varying concentrations of proteoglycans (versican, biglycan, and decorin), hyaluronan, and collagen (types I and III).[25] The ECM modulates important events within the developing neointima, including cell proliferation, migration, growth factor expression, and remodeling.[26] And ECM accounts for > 50% of the volume of neointimal restenosis lesions.[26] In autopsy coronary arteries, post-PCI lesions at healing stage show the accumulation not only of collagen type I, decorin and biglycan but also of versican and hyaluronan at least for 18 months, suggesting the requirement of a long time for complete healing. But, it is reported that versican and hyarulonan decreases with an increase in collagen type III content as time goes by.[27]

In the present study, even in de novo lesions, myxomatous ECM was frequently found, which was usually found in restenosis lesion after PCI, and rich proteoglycans, suggesting the possibility of previous plaque rupture before PCI. The present study with the result of a tendency of increased myxomatous tissue in restenosis group, suggests that myxomatous ECM shows ongoing intimal proliferation and potency to restenosis. Moreover, in myxomatous ECM, we observed elevated immunoreactivity to matrix metalloproteinases-1, 2 and 9, which may play an prominent role in plaque destabilization and coronary restenosis after PCI.

SMCs

In this study, SMCs content was similar in the two groups (restenosis/no restenosis), suggesting that the severity of vascular narrowing after coronary atherectomy was not related to the intimal SMC content in the culplit lesion.

The previous analysis of the intima revealed that α-SMA positive cells were quite numerous; however, they had lost smooth muscle myosin heavy chains (SM-MHCs) expression very importantly and smoothelin expression almost completely. These features support the assumption that in all the situations examined intimal SMCs have acquired the myofibroblastic phenotype. SM-MHCs/α-SMA, ie, as a value representative of SMC differentiation level, was lower in stable plaques and erosions with > 75% cross-sectional luminal narrowing compared with mildly stenotic plaques.[28] It means that SMCs of the culplit lesions with the high degree of lesions severity in our study are differentiated from those in mildly stenotic lesions, suggesting that deep dissection evoked by PCI caused phenotypic modulation of medial SMCs to synthetic state and their proliferation.

Cholesterol gruel

There was a tendency toward larger area occupied by cholesterol gruel in restenosis group. It may depend on necrotic core size. Plaque size cannot be evaluated by DCA. However, larger plaque size may include larger necrotic core. The previous studies reported linear associations between plasma cholesterol level and coronary restenosis. One of the studies provides evidence for the critical role of cholesterol dependent oxidant stress in the pathophysiology of restenosis after PTCA.[29] In our study, cholesterol gruel may induce coronary restenosis in the same mechanism.

Even in the current era of drug-eluting stents, restenosis at the proximal edge was the cause of about two thirds the cases of restenosis, possibly due to plaque compression and distribution along the vessel rather than intimal hyperplasia.[30] Given the possible role of plaque shifting at the edges of a stent in causing restenosis, debulking could be added to the local drug effect in complex le-

sions.

Study Limitations

The lesions we can perform DCA are limited to relatively large proximal coronary segments. Loss of expression of α-actin in SMCs is associated with a phenotypic change from a contractile to a "synthetic" phenotype, and specific markers of activated SMCs were not evaluated in every sample. The weight of retrieved samples was not measured correctly, then we did not show the data.

Conclusion

In de novo lesions, atherectomy specimens reflect the heterogeneity of features that are found in plaques. Macrophages infiltration, calcified fragments, cholesterol rich gruel and myxomatous ECM might be predictors of restenosis after directional coronary atherectomy, suggesting a possible role of them in restenotic process after PCI even in de novo lesion.

Disclosures

none

REFERENCES

1) Wight TN, Merrilees MJ. Proteoglycans in atherosclerosis and restenosis: key roles for versican. Circ Res. 2004 ; **94**: 1158–67. Review.
2) Currier JW, Faxon DP. Restenosis after percutaneous transluminal coronary angioplasty: have we been aiming at the wrong target? J Am Coll Cardiol. 1995; **25**: 516–20.
3) Glover C, Ma X, Chen YX, Miller H, Veinot J, Labinaz M, et al. Human in-stent restenosis tissue obtained by means of coronary atherectomy consists of an abundant proteoglycan matrix with a paucity of cell proliferation. Am Heart J. 2002; **144**: 702–9.
4) Rodriguez A, Santaera O, Larribau M, Fernandez M, Sarmiento R, Perez-Balino N, et al. Coronary stenting decreases restenosis in lesions with early loss in luminal diameter 24 hours after successful PTCA. Circulation. 1995; **91**: 1397–402.
5) Schwartz SM, deBlois D, O'Brien ERM. The intima: soil for atherosclerosis and restenosis. Circ Res. 1995; **77**: 445–65.
6) Hoshino Y, Kurabayashi M, Kanda T, Hasegawa A, Sakamoto H, Okamoto E, et al. Regulated expression of the BTEB2 transcription factor in vascular smooth muscle cells: analysis of developmental and pathological expression profiles shows implications as a predictive factor for restenosis. Circulation. 2000; **102**: 2528–34.
7) Sakamoto H, Sakamaki T, Kanda T, Hoshino Y, Sawada Y, Sato M, et al. Smooth muscle cell outgrowth from coronary atherectomy specimens in vitro is associated with less time to restenosis and expression of a key Transcription factor KLF5/BTEB2. Cardiology. 2003; **100**: 80–5.
8) Ishikawa T, Hatakeyama K, Imamura T, Date H, Shibata Y, Hikichi Y, et al. Involvement of C-reactive protein obtained by directional coronary atherectomy in plaque instability and developing restenosis in patients with stable or unstable angina pectoris. Am J Cardiol. 2003; **91**: 287–92.
9) Moreno PR, Bernardi VH, Lopez-Cuellar J, Newell JB, McMellon C, Gold HK, et al. Macrophage infiltration predicts restenosis after coronary intervention in patients with unstable angina. Circulation. 1996; **94**: 3098–102.
10) Meuwissen M, Piek JJ, van der Wal AC, Chamuleau SAJ, Koch KT, Teeling P, et al. Recurrent unstable angina after directional coronary atherectomy is related to the extent of initial coronary plaque inflammation. J Am Coll Cardiol. 2001; **37**: 1271–6.
11) Dangas G, Fuster V. Management of restenosis after coronary intervention. Am Heart J. 1996; **132**: 428–36.
12) Ishiwata S, Nakanishi S, Nishiyama S, Seki A. Cause of coronary events after successful coronary angioplasty. Coron Artery Dis. 1996; **7**: 573–7.
13) Libby P, Schwartz D, Brogi E, Tanaka H, Clinton S. A cascade model for restenosis. Circulation. 1992; **86**(suppl III) : III47–III52. 18.
14) Cole CW, Makhoul RG, McCann RL, O Malley MK, Hagen PO. A neutrophil derived factor(s) stimulates [3H]thymidine incorporation by vascular smooth muscle cells in vitro. Clin Invest Med. 1988; **11**: 62–7.
15) Morimoto S, Mizuno Y, Hiramitsu S, Yamada K, Kubo N, Nomura M, et al. Restenosis after percutaneous transluminal coronary angioplasty: A histopathological study using autopsied hearts. Jpn Circ J. 1990; **54**: 43–56.
16) Mintz GS, Popma JJ, Pichard AD, Kent KM, Satler LF, Wong SC, et al. Arterial remodeling after coronary angioplasty: A serial intravascular ultrasound study. Circulation. 1996; **94**: 35–43.
17) Wilensky RL, March KL, Gradus-Pizlo I, Sandusky G, Fineberg N, Hathway DR. Vascular injury, repair and restenosis after percutaneous transluminal angioplasty in the atherosclerotic rabbit. Circulation. 1995; **92**: 2995–3005.
18) Zempo N, Koyama N, Kenagy RD, Lea HJ, Clowes AW. Regulation of vascular smooth muscle cell migration and proliferation in vitro and in injured rat arteries by a synthetic matrix metalloproteinase inhibitor. Arterioscler Thromb Vasc Biol. 1996; **16**: 28–33.
19) Michelle P, Colleen I, Reidy MA. Inhibition of matrix

metalloproteinase activity inhibits smooth muscle cell migration but not neointimal thickening after arterial injury. Circ Res. 1996; **78**: 38–43.
20) Falk E, Shah PK, Fuster V. Coronary plaque disruption. Circulation. 1995; **92**: 657–71.
21) Kruntz RL, Hinohara T, Safian RD, Selmon MR, Simpson JB, Baim DS. Restenosis after directional coronary athelectomy: Effects of luminal interventions in 413 lesions. Circulation. 1992; **86**: 1394–9.
22) Fishman RF, Kruntz RE, Carrazza JP Jr, Miller MJ, Senerchia CC, Schnitt SJ, et al. Long term results of directional coronary athelectomy: Predictors of restenosis. J Am Coll Cardiol. 1992; **20**: 1101–10.
23) Fukuda A, Kitayama M, Takekoshi N. Plaque reduction and restenosis in coronary athelectomy. J Jpn Coll Angiol. 2004; **44**: 59–68.
24) Hay ED. Cell Biology of Extracellular Matrix. New York, NY: Plenum Press; 1991.
25) Garratt KN, Edwards WD, Kaufmann UP, Vlietstra RE, Holmes DR Jr. Differential histopathology of primary atherosclerotic and restenotic lesions in coronary arteries and saphenous vein bypass grafts: analysis of tissue obtained from 73 patients by directional atherectomy. J Am Coll Cardiol. 1991; **17**: 442–8.
26) Schwartz RS, Holmes DR Jr, Topol EJ. The restenosis paradigm revisited: an alternative proposal for cellular mechanisms. J Am Coll Cardiol. 1992; **20**: 1284–93.
27) Farb A, Kolodgie FD,Hwang JY, Burke AP, Tefera K, Weber DK, Wight TN, et al. Extracellular matrix changes in stented human coronary arteries: Circulation. 2004; **110**: 940–7.
28) Hao H, Gabbiani G, Camenzind E, Bacchetta M, Virmani R, Bochaton-Piallat ML. Phenotypic modulation of intima and media smooth muscle cells in fatal cases of coronary artery lesion. Arterioscler Thromb Vasc Biol. 2006; **26**: 326–32.
29) Zee RY, Fernandez-Otiz A, Macaya C, Pintor E, Lindpaintner K, Fernandez-Cruz A. High preprocedural non-HDL cholesterol is associated with enhanced oxidative stress and monocyte activation after coronary angioplasty: possible implications in restenosis. Heart. 2003; **89**: 773–9.
30) Holmes DR Jr, Leon MB, Moses JW, Popma JJ, Cutlip D, Fitzgerald PJ, et al. Analysis of 1-year clinical outcomes in the SIRIUS trial: a randomized trial of a sirolimus-eluting stent versus a standard stent in patients at high risk for coronary restenosis. Circulation. 2004; **109**: 634–40.

Eur J Nucl Med Mol Imaging (2010) 37:377–385
DOI 10.1007/s00259-009-1262-2

ORIGINAL ARTICLE

Quantification of regional myocardial oxygen metabolism in normal pigs using positron emission tomography with injectable ^{15}O-O_2

Takashi Temma · Hidehiro Iida · Takuya Hayashi · Noboru Teramoto · Youichiro Ohta · Nobuyuki Kudomi · Hiroshi Watabe · Hideo Saji · Yasuhiro Magata

Received: 27 April 2009 / Accepted: 10 August 2009 / Published online: 4 September 2009

Abstract
Purpose Although ^{15}O-O_2 gas inhalation can provide a reliable and accurate myocardial metabolic rate for oxygen by PET, the spillover from gas volume in the lung distorts the images. Recently, we developed an injectable method in which blood takes up ^{15}O-O_2 from an artificial lung, and this made it possible to estimate oxygen metabolism without the inhalation protocol. In the present study, we evaluated the effectiveness of the injectable ^{15}O-O_2 system in porcine hearts.
Methods PET scans were performed after bolus injection and continuous infusion of injectable ^{15}O-O_2 via a shunt between the femoral artery and the vein in normal pigs. The injection method was compared to the inhalation method. The oxygen extraction fraction (OEF) in the lateral walls of the heart was calculated by a compartmental model in view of the spillover and partial volume effect.
Results A significant decrease of lung radioactivity in PET images was observed compared to the continuous inhalation of ^{15}O-O_2 gas. Furthermore, the injectable ^{15}O-O_2 system provides a measurement of OEF in lateral walls of the heart that is similar to the continuous-inhalation method (0.71 ± 0.036 and 0.72 ± 0.020 for the bolus-injection and continuous-infusion methods, respectively).
Conclusion These results indicate that injectable ^{15}O-O_2 has the potential to evaluate myocardial oxygen metabolism.

Keywords Myocardial oxygen metabolism · PET · Pig · OEF · Injectable ^{15}O-O_2

T. Temma · H. Saji
Department of Patho-Functional Bioanalysis,
Graduate School of Pharmaceutical Sciences, Kyoto University,
Kyoto, Japan

H. Iida · T. Hayashi · N. Teramoto · Y. Ohta · N. Kudomi · H. Watabe
Department of Investigative Radiology,
National Cardiovascular Center Research Institute,
Osaka, Japan

Y. Magata (✉)
Laboratory of Genome Bio-Photonics,
Photon Medical Research Center,
Hamamatsu University School of Medicine,
1-20-1 Handayama,
Hamamatsu 431-3192, Japan
e-mail: magata@hama-med.ac.jp

Introduction

In the myocardium, fatty acid or glucose is used to produce energy by aerobic metabolism. Oxygen is one of the most important substrates closely related to the aerobic metabolism in the TCA cycle; thus, oxygen metabolism should be a direct reflection of myocardial metabolism of these substrates. Therefore, there has been considerable interest in the development of a method to quantify oxygen metabolism in the myocardium.

Recently, ^{11}C-acetate has been used for this purpose [1–5]. ^{11}C-acetate is taken up by the mitochondria and metabolically converted into acetyl-CoA. It then enters the TCA cycle and is transformed to ^{11}C-CO_2, which is cleared rapidly from the myocardium. Thus, the clearance pharmacokinetics reflects oxygen metabolism in the myocardium. However, the quantification of oxygen metabolism using ^{11}C-acetate is quite difficult because of various intermediary compounds.

The use of ^{15}O-O_2 gas inhalation and PET scanning can provide a quantitative myocardial metabolic rate for oxygen ($MMRO_2$) [6, 7]. The tracer kinetic model used is based on that originally proposed to describe the behavior of ^{15}O-O_2 in brain tissue [8, 9]. However, the direct translation of the

compartmental model for the brain to the heart is not permitted, because subtraction for spillover from gas volume in addition to that from the blood pool is needed. A previous study demonstrated that the gas volume can be accurately estimated from the transmission scan data; thus, this technique did not require additional emission scanning for estimating the quantitative gas volume images [6, 7]. However, gaseous radioactivity in the lung during the inhalation of ^{15}O-O_2 gas is too high in comparison to other regions. Subtraction for this contribution is straightforward and accurate using the transmission scan-derived gaseous volume images, but the lung radioactivity degraded image quality in the estimated $MMRO_2$ images.

As an alternative to gas inhalation, we recently developed a method to prepare an injectable form of ^{15}O-O_2. This was accomplished by exposing pre-collected blood to ^{15}O-O_2 gas using a small artificial lung system resulting in a maximum yield of 130 MBq/ml. We demonstrated that cerebral oxygen metabolism could be estimated in normal and ischemic rats using injectable ^{15}O-O_2 [10–12]. This technique has the potential of avoiding the inhalation protocol.

The aim of the present study was therefore to test the feasibility of using the injectable ^{15}O-O_2 oxygen system for estimating myocardial oxygen metabolism in pigs. The injection method was compared to the inhalation method to determine if the injection method resulted in a reduction of lung radioactivity, an improved image quality, a more accurate estimate of myocardial oxygen metabolism, and an improved signal-to-noise ratio.

Materials and methods

Theory

^{15}O-Oxygen was administered by IV injection or inhalation and was carried as ^{15}O-hemoglobin by blood to peripheral tissues including the myocardium, where it was converted to ^{15}O-water (^{15}O-H_2O_{met}) through aerobic metabolism. The increased distribution volume of ^{15}O-H_2O_{met}, represented by the exchangeable water space of tissue, causes delayed removal of radioactivity. This allows the definition of an appropriate model and equations to be derived for the calculation of a regional myocardial metabolic rate for oxygen ($rMMOR_2$) and regional oxygen extraction fraction (rOEF). Previous studies demonstrated that these calculations were similar to those used for estimating cerebral blood flow and oxygen metabolism and require the measurement of regional myocardial blood flow (rMBF) and a correction for spillover of activity from the vascular pools and the pulmonary alveoli [6, 7]. rMBF was measured by the ^{15}O-H_2O injection technique [13]. Activity in the vascular pools of the heart chambers and the lung was evaluated with a conventional measurement of blood volume using ^{15}O-CO, and activity in the pulmonary alveoli was evaluated with an unconventional and indirect measurement of gas volume obtained from the transmission scan. Furthermore, the existence of recirculating ^{15}O-H_2O_{met} in the blood freely accessible to the myocardium was taken into consideration.

The differential equation describing the myocardial kinetics after administration of ^{15}O-O_2 can be written as follows:

$$\frac{dC^{myo}(t)}{dt} = OEF \cdot f \cdot A_o(t) + f \cdot A_w(t) - \left(\frac{f}{p} + \lambda\right) C^{myo}(t) \quad (1)$$

where $C^{myo}(t)$ designates the true radioactivity concentration in the myocardium at time t, f is myocardial blood flow, $A_O(t)$ is the ^{15}O-O_2 radioactivity concentration in arterial blood, $A_W(t)$ is the ^{15}O-H_2O radioactivity concentration in arterial blood, p is the myocardium/blood partition coefficient of water, and λ is the physical decay constant of O-15.

Solving Eq. (1) in terms of $C^{myo}(t)$ gives:

$$C^{myo}(t) = OEF \cdot f \cdot A_o(t) * e^{-\left(\frac{f}{p}+\lambda\right)\cdot t} + f \cdot A_w(t) * e^{-\left(\frac{f}{p}+\lambda\right)\cdot t} \quad (2)$$

where the asterisk denotes the convolution integral. During steady-state conditions under the continuous administration of ^{15}O-O_2, the following relationship holds:

$$C^{myo} = \frac{OEF \cdot f \cdot A_o + f \cdot A_w}{\left(\frac{f}{p} + \lambda\right)} \quad (3)$$

In the actual PET studies, the spillover from vascular pools and pulmonary alveoli and the partial volume effect should be taken into consideration [14]. Then, the measured radioactivity concentration in the region of interest (ROI) in the myocardium ($R^{myo}(t)$) can be expressed as:

$$\begin{aligned} R^{myo}(t) = {} & \alpha \cdot C^{myo}(t) \\ & + (V_B^{myo} \cdot A_t(t) - \alpha \cdot F_{Vein} \cdot OEF \cdot A_o(t) - \alpha \cdot F_{Vein} \cdot A_w(t)) \\ & + V_G^{myo} \cdot C_{gas}(t) \end{aligned} \quad (4)$$

where α denotes the myocardial tissue fraction, V_B^{myo} is the myocardial blood volume, $A_t(t)$ is the total O-15 radioactivity concentration in arterial blood, F_{vein} is the microscopic venous blood volume, V_G^{myo} is the gas volume in the myocardial ROI and $C_{gas}(t)$ is the O-15 radioactivity concentration in V_G^{myo}.

With the bolus injection or infusion methods using an artificial lung system, the radioactivity in the pulmonary alveoli is expected to be negligible in comparison with the inhalation method. Thus, Eq. (4) can be converted to:

$$R^{myo}(t) = \alpha \cdot C^{myo}(t) + (V_B^{myo} \cdot A_t(t) - \alpha \cdot F_{Vein} \cdot OEF \cdot A_o(t) - \alpha \cdot F_{Vein} \cdot A_w(t)) \quad (5)$$

Subjects

In this study, four healthy miniature pigs (22–30 kg) were used. The pigs were anesthetized by IM injection of ketamine and xylazine followed by continuous infusion of propofol (5 mg/kg/h). The animals were then placed in the supine position on the bed of the PET scanner. All experimental procedures were approved by the local animal welfare committee.

Injectable ^{15}O-O_2 preparation

In the "injection" study, injectable ^{15}O-O_2 was used. Injectable ^{15}O-O_2 was prepared as described previously [10–12]. In brief, part of an infusion line kit (Terumo Corporation, Tokyo, Japan) and an artificial lung 18 cm in length (Senko Medical Instrument Mfg Co. Ltd., Tokyo, Japan) were connected using silicone tubing to make a closed system. Then, venous blood collected from a pig, which was used in the following PET studies, was added to the system and circulated (100 ml/min) by a peristaltic pump, followed by introduction of ^{15}O–O_2 gas (~7,000 MBq/min/433 ml) into the artificial lung for 15 min to prepare injectable ^{15}O-O_2 (5.6–60.7 MBq/ml).

In the "continuous infusion" study, the left femoral artery and right femoral vein were both cannulated. The two cannulas from the artery and the vein were connected to the opposite sides of an artificial lung to create a femoral shunt. The blood flow in the shunt was aided by a peristaltic pump (30–50 ml/min). ^{15}O-O_2 gas (~7,000 MBq/min/433 ml) was continuously introduced into the artificial lung.

PET protocol (Fig. 1)

The PET scanner was an ECAT EXACT HR (CTI/Siemens) [15], which has an imaging field of view (FOV) of 55 cm in diameter and 15 cm in axial length. The spatial resolution of the scanner is 5.8 mm in full width at half maximum at the center of the FOV.

After obtaining a 20-min transmission scan for attenuation correction and gas volume estimation, the blood pool image was obtained with a 4-min PET scan after the pigs inhaled 2.7 GBq ^{15}O-CO for 30 s. Arterial blood samples were taken every minute during the ^{15}O-CO scanning, and

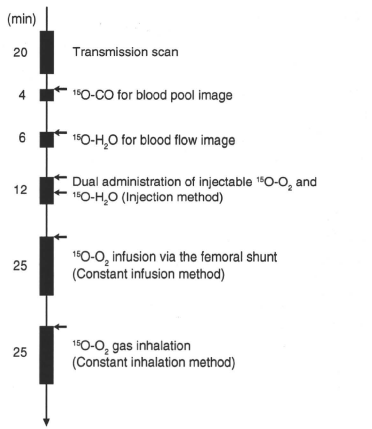

Fig. 1 Outline of the PET imaging study. The interval between scans was more than 15 min to allow for physical decay of O-15 radioactivity to background levels

the radioactivity concentration in the whole blood was measured with a NaI well-type scintillation counter calibrated against the PET scanner. Subsequently, ^{15}O-water was injected into the right femoral vein for 30 s at an infusion rate of 10 ml/min (injected radioactivity was about 1.11 GBq). Immediately after injection of ^{15}O-water, 26 dynamic frames (12×5 s, 8×15 s and 6×30 s) of PET data were acquired for 6 min.

Furthermore, two PET scans were successively performed after the IV injection of ^{15}O-O_2 (5.6–60.7 MBq/ml) for 30 s at an injection rate of 20–80 ml/min for the "injection" study, and by the continuous ^{15}O-O_2 gas infusion through the artificial lung in the femoral shunt for the "continuous infusion" study. In the "injection" study, 52 dynamic frames (12×5 s, 8×15 s, 6×30 s, 12×5 s, 8×15 s and 6×30 s) of PET data were acquired for 12 min, and 1.11 GBq of ^{15}O-water was injected IV for 30 s at 10 ml/min starting at 6 min after the administration of IV ^{15}O-O_2 according to the dual administration protocol we developed previously [16]. In the "continuous infusion" study, 26 dynamic frames (10×30 s, 5×60 s, 1×600 s and 10×30 s) were acquired for 25 min, and the 600-s frame was used for steady-state analysis.

Another PET scan was performed by ^{15}O-O_2 gas inhalation in one of the four pigs in the same protocol as the "continuous infusion" study. This was the "continuous inhalation" study. The interval between scans was more